Vibration Isolation Mechanism of Row Piles Under Single-Point Excitation

Jing-lei Liu, Rui-heng Zhang, Xiao-yu Zhao and Huan Liu

Abstract To study the vibration isolation mechanism of row piles exposed to vibrations generated at a single point, a finite element model of a foundation using infinite element boundaries is established based on the theory of an elastic half-space body. The model included a single-point vibration source in the free field and piles arranged in a row, and corresponding contour maps of the amplitude dissipation ratio (Ar) were drawn. The results show that the vibration waves radiate out from the excitation point and that their acceleration amplitude decays continuously. The overall vibration isolation progressively improves as the number of piles and the row depth increase. However, the degree of improvement in the isolation effect decreases with increasing depth. If the spacing between row piles is too large, the vibration isolation effect of the row piles will be unsatisfactory. However, reducing the row spacing does not necessarily improve the vibration isolation effect of row piles. Compared with a hollow pile, a solid pile has a better vibration isolation effect, but the difference is not significant. Additionally, the vibration isolation effect of a circular pile is worse than that of a square pile. As the distance between the vibration source and the row piles decreases, the isolation effect becomes more pronounced, but the difference is not pronounced. Furthermore, the isolation effect of row piles is better for low-frequency vibrations than for intermediate- and high-frequency vibrations.

Keywords Vibration isolation · Row piles · Mechanism analysis · Infinite boundary · Finite element analysis

J. Liu (✉) · R. Zhang · X. Zhao · H. Liu
School of Civil Engineering, Hebei University of Architecture, Zhangjiakou 075000, Hebei, China
e-mail: kingbest_1118@163.com

E. Tutumluer et al. (eds.), *Advances in Environmental Vibration and Transportation Geodynamics*, Lecture Notes in Civil Engineering 66,
https://doi.org/10.1007/978-981-15-2349-6_3

1 Foreword

With the rapid development of modern industry and accelerating urbanization, contamination from various types of environmental vibrations has received widespread public attention [1–3]. International organizations have listed vibration pollution as one of the seven major environmental hazards in the world [4].

Currently, vibration pollution control is one of the most important topics being investigated by scholars in China and abroad [5, 6]. Yang et al. [7] suggested that installing vibration isolation barriers in foundation soil can effectively control environmental vibration pollution. Woods [8] studied a discontinuous insulation barrier and proposed that the pile diameter of a single-row pile isolation barrier should be greater than one-sixth the wavelength of the barrier. Andersen and Nielsen [9] studied empty and filled trenches and found that empty trenches are more effective isolation barriers. Furthermore, a combined barrier involving both empty trenches and row piles is more effective than using a single isolation barrier alone. Aviles and Sanchez-Sesma [10, 11] studied the scattering effect of single-row piles on an SH wave and showed that the vibration isolation effect of a rigid pile is better than that of a flexible pile. Hayakawa [12] studied the mechanism and propagation laws of vibration waves and proposed a prediction method for environmental vibration levels. Xu et al. [13] and Xia et al. [14] studied the effects on the vibration isolation of various forms of barriers with respect to SV waves and proposed that the vibration isolation effect of discontinuous hollow pipe pile barriers increases with decreasing pile spacing, providing a basis for practical applications. Shi and Gao [15] used a semi-analytic boundary element method to study the vibration isolation of far-field single-row piles in saturated soils. These researchers concluded that increasing the pile length, pile diameter and pile shear modulus effectively improves the vibration isolation effect of row piles. Ba et al. [16] considered the influence of the track and layered foundations and studied the vibration isolation effect of empty trenches on a foundation using the 2.5-dimensional indirect boundary element method. They concluded that different foundation models, the depth of the empty trenches and the distance between the empty trenches and the foundation impact the vibration isolation effect. Chen and Huang [17] studied the vibration isolation effect of filled trenches for traffic vibrations in viaducts and concluded that ring-shaped filled trenches can achieve a good vibration isolation effect. Feng et al. [18] and Zhang et al. [19] used model tests to analyze the vibration isolation effects of typical vibration isolation barriers, such as empty trenches, filled trenches and row piles, and these researchers obtained results that are beneficial to engineering practice.

These results demonstrate that various types of vibration isolation barriers can help mitigate vibration pollution, and we describe studies on the effects of vibration isolation factors associated with vibration isolation barriers. Most of these studies examined points or lines behind the isolation barrier, but few studies have examined

the sources of vibrations and planes within a certain range around the barrier. Therefore, to objectively describe the vibration isolation effect of a row pile system in a plane within a certain range subjected to single-point vibration, we compare the vertical acceleration at the ground surface at points where no vibration isolation measures are available to that at points where row pile vibration isolation is available to determine the surface amplitude dissipation ratio (Ar). Additionally, this work creates a corresponding Ar contour map, determines the effect of different factors on the vibration isolation effect over a certain range and acts as a reference for research on vibration and vibration isolation.

2 Vibration Isolation Principle

When operating a train, track irregularities, orbital seams, and wheel and track interactions generate a reciprocating load at a certain speed, which is transmitted to and propagates through the surrounding soil, vibrating the soil. This process is the main cause of vibrations in rail transit systems. Because of its small dynamic strain, this vibration appears as an elastic wave in the soil. Therefore, for rail transit vibrations, the soil can be analyzed as an elastic half-space body. Jiang et al. [20] numerically calculated the integral expression of the half-space body response and obtained the response and surface displacement of all points inside the elastic half-space body. A vibration wave propagates in the soil in the form of a body wave and a surface wave. The vibration wave propagates along the surface of the soil, mainly in the form of a surface wave, and the main component of the surface wave is a Rayleigh wave. Rayleigh waves are surface waves that propagate at a one-time wavelength depth. The decay rate of the wave is slow, causing the ground to vibrate violently. Because of the large difference in the impedance ratio between a vibration isolation barrier and the soil, vibration isolation measures placed in the transmission path of a vibration wave can block the vibration wave. A vibration wave advances in a uniform medium without changing direction. When the vibration wave encounters an obstacle, it is decomposed into a reflected wave, a diffracted wave and a transmitted wave. This effect is the basic mechanism responsible for the shielding effect of a barrier.

3 Verifying the Validity of Finite Element Analysis

To verify the effectiveness of finite element analysis for vibration-related fields, model tests were conducted, and finite element models of the same size as the model tests were established. The results were compared to ensure that the results of the finite element analysis are consistent with the actual results.

3.1 Model Test Overview

The model test used an outdoor square sand pit with a length × width × height of 3.0 × 2.0 × 1.5 m filled with 98% sand with a grain size distribution ranging from 1.75 to 0.075 mm. The soil moisture content was maintained at 9–10%. The soil mass was layered and compacted. The soil density was 1700–1800 kg/m^3. The test adopted a WS-Z30 shaking table control system. The equipment mainly included a data acquisition controller, a power amplifier, a charge amplifier, an exciter, a signal generator, an accelerometer amplifier and an acceleration sensor.

The row piles were fabricated from C30 concrete with a square cross section, with cross-sectional dimensions of 10.0 × 10.0 cm and a height of 40 cm. The first pile was positioned at the geometric center of the row pile test site, and the other piles were arranged at 15 cm intervals in the transverse direction. The exciter used in the experiment was positioned 90 cm in front of the central pile. The test used four accelerometers on the soil surface along the longitudinal axis to collect vertical acceleration data from the soil itself. Sensor #1 was placed 10 cm in front of the row piles, and sensors #2–4 were placed 10 cm, 20 cm and 50 cm behind the row piles, respectively. The pile and sensor layout are shown in Fig. 1. For the experiment, a sine wave with an excitation frequency of 10 Hz was selected, and a sampling frequency of 5000 times/s was used with a sampling time of 10 s. During this period, the charge amplifier values needed to be consistent.

3.2 Finite Element Model Overview

3.2.1 Model Size and Boundary Settings

In this paper, a three-dimensional model is used for calculation, and a finite element model of the same size as the model test is established. To prevent the model from acting as a fixed boundary and causing vibration wave reflection, an infinite element is used as the perimeter and the bottom boundary. Therefore, the CIN3D8 infinite element is used for the surrounding and bottom elements of the model, while the other parts use the finite element C3D8R three-dimensional stress element. The finite element model is shown in Fig. 2.

3.2.2 Model Material Parameters and Load Selection

The model soil and pile material parameters are shown in Table 1. The three-dimensional stress element uses sand properties, and the surrounding and bottom infinite elements use soil properties to simulate the actual situation of the test site more accurately.

The test uses an excitation frequency of 10 Hz. The vibration load includes a static load and a dynamic load, as shown in Eq. (1):

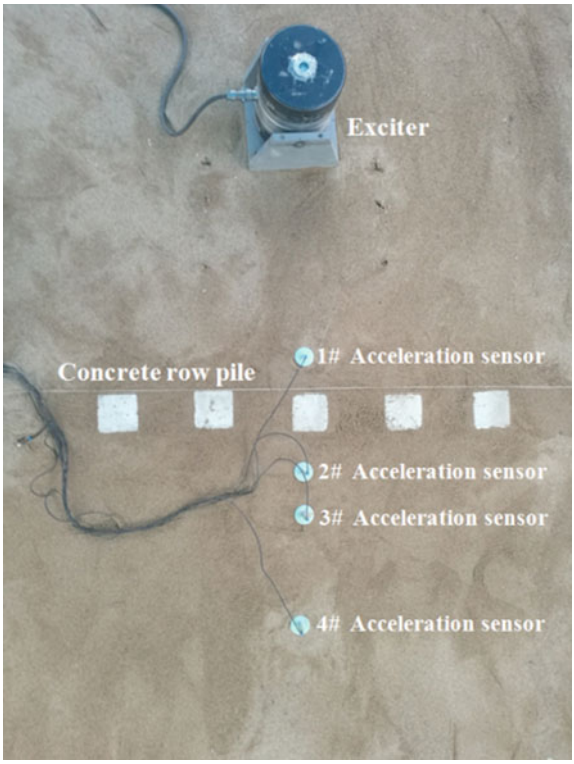

Fig. 1 Layout of concrete pile and sensor

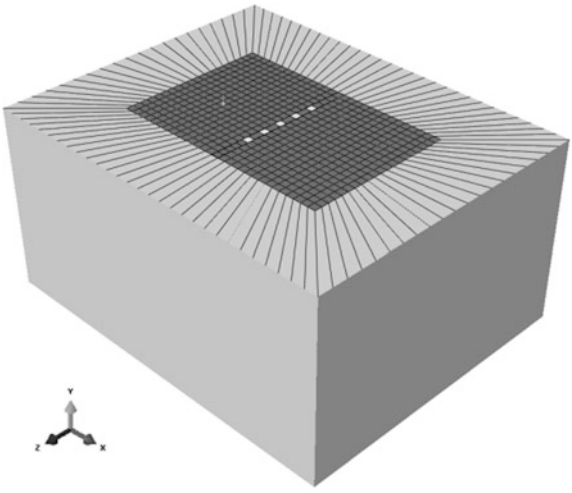

Fig. 2 FE model corresponding to the size of the experiment

Table 1 Material parameters

Type	Density (kg m^{-3})	Elastic modulus (Pa)	Poisson's ratio	α	β
Sand	1750	2.00E+07	0.3	0.406	0.072
Soil	1900	2.00E+07	0.3	0.406	0.072
Pile	2200	2.20E+10	0.2	0.112	0.020

$$F(t) = P_0 + P_1 \sin(\omega_1 t) \tag{1}$$

where P_0 (kN) is the exciter's weight, P_1 (kN) is the dynamic load peak, and ω_1 is the vibration circle frequency.

According to the experimental data, the excitation function is shown in Eq. (2).

$$F(t) = 0.25 + 0.08 \sin 62.8t \tag{2}$$

3.3 Comparison of Results

3.3.1 Data Processing Method

The row pile vibration isolation effect is expressed using Ar. The expression is shown in Eq. (3), and the smaller the value of Ar is, the better the vibration isolation effect [17].

$$Ar = \frac{a_1}{a_0} \tag{3}$$

In the above equation, a_1 is the acceleration value with vibration isolation measures, and a_0 is the acceleration value without vibration isolation measures.

3.3.2 Comparison of the Model Test and FE Calculation Results

To verify the reliability of the finite element analysis calculation, a model of the same size as the finite element model was used for comparison with the finite element model. In the calculation of the model test and the finite element model, two isolation schemes, i.e., no vibration isolation measures and row pile vibration isolation (section size: 5.0 cm; depth: 40.0 cm; pile spacing: 15.0 cm), were used. A vibration force at a frequency of 10 Hz was used, and the test results are expressed as vertical acceleration.

Figure 3 and Table 2 show the soil acceleration values and amplitude dissipation ratio for the model test and the finite element analysis for two conditions. In the model test and the finite element analysis, the vertical acceleration at a distance of

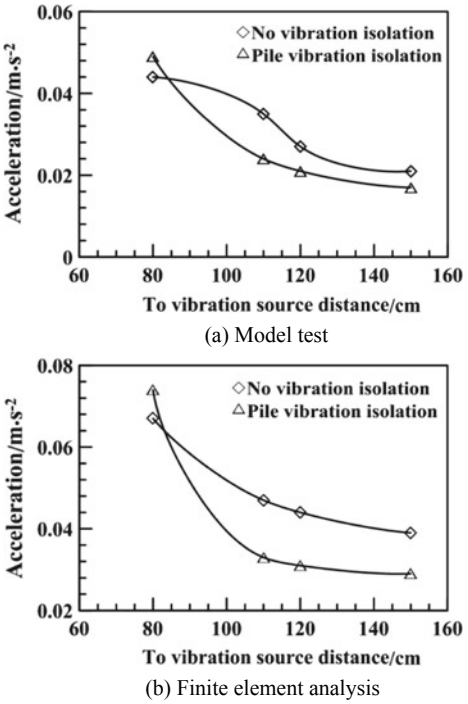

Fig. 3 Changes in acceleration as a function of distance

Table 2 Comparison of the acceleration for the two conditions

Vibration source distance (cm)	Model test			Finite element analysis		
	Acceleration (m s^{-2})		Amplitude dissipation ratio (*Ar*) (%)	Acceleration (m s^{-2})		Amplitude dissipation ratio (*Ar*) (%)
	No vibration isolation measures	Row pile vibration isolation		No vibration isolation measures	Row pile vibration isolation	
80	0.067	0.074	110.45	0.044	0.049	111.36
110	0.047	0.033	70.21	0.035	0.024	68.57
120	0.044	0.031	70.45	0.027	0.021	77.78
150	0.039	0.029	74.36	0.021	0.017	80.95

80 cm from the vibration source increased after the isolation barrier was set; the amplitude dissipation ratios were 111.36 and 110.45%, respectively. This effect is observed because a reflected wave is generated at the front of the piles in the isolation barrier, which increases the vertical acceleration. In the model test and finite element analysis, the amplitude dissipation ratios of the measurement points behind the isolation barrier were 70.21–74.36 and 68.57–80.95%, respectively. Thus, the accelerations were lower by 19.05–31.43 and 25.64–29.79%,

respectively. There is a better vibration isolation effect within a certain range of the row pile. The model test is consistent with finite element analysis in terms of regularity. In summary, finite element analysis reflects the effectiveness of the vibration isolation barrier and verifies its feasibility for predicting vibration isolation effects.

4 Establishing the Finite Element Model and Design Scheme

4.1 Establishing the Finite Element Model

4.1.1 Model Size and Boundary Settings

This study uses ABAQUS software to create a three-dimensional model for the calculations. The model surface layout is shown in Fig. 4.

The model is based on the theory of an elastic half-space body. To prevent the model from requiring a fixed boundary and causing the reflection of any vibration waves, an infinite boundary is used as the surrounding and bottom boundaries. The length, width and height of the model are 50 m, 50 m and 30 m, respectively. A CIN3D8 infinite element with a thickness of 10 m is used for the surrounding and bottom units; other parts use a C3D8R three-dimensional stress unit with dimensions of 30 × 30 × 20 m. To prevent the infinite boundary from affecting the surroundings, 5 m finite element units are left as transitional areas. The constant value line drawing area is centered at 20 × 20 m. The finite element calculation model is shown in Fig. 5.

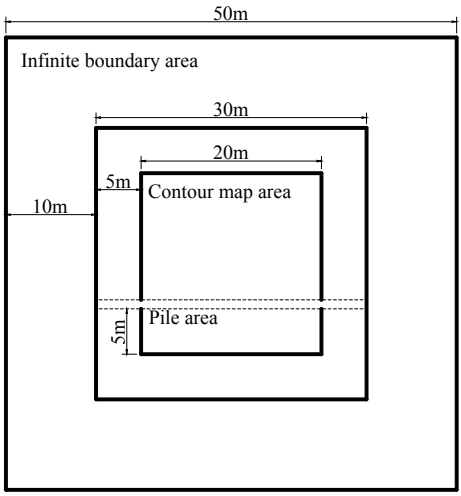

Fig. 4 Model surface layout

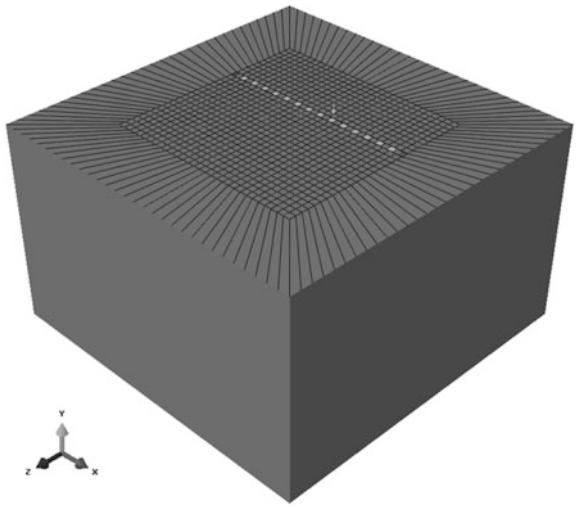

Fig. 5 Finite element calculation model

4.1.2 Model Material Parameters

The model was calculated using elastic materials. The model material parameters are shown in Table 3.

Because the vibration waves are attenuated in the soil and piles, it is necessary to provide damping to the soil and piles. The model uses Rayleigh damping in ABAQUS to define the damping of soil and piles. For the soil, the mass damping coefficient α is 0.406, and the stiffness damping coefficient β is 0.072. For the pile–soil system, the mass damping coefficient α is 0.112, and the stiffness damping coefficient β is 0.020.

4.1.3 Vibration Load Setting

Single-point vibration excitation is used to generate the vibration. The vibration uses a simple harmonic wave. A vibration force function is used to simulate the vibration load, which includes a static load simulation of the total vibration source weight and a dynamic load to simulate a source vibration. The expression is shown in Eq. (4):

$$F(t) = P_0 + P_1 \sin(\omega_1 t) \tag{4}$$

Table 3 Model material parameters

Type	Density (kg m^{-3})	Elastic modulus (Pa)	Poisson's ratio
Soil	1900	2.00E+07	0.300
Pile	2500	2.20E+10	0.200

Table 4 Vibration wave amplitude in different frequency bands

Frequency	Amplitude α_1 (mm)
Low frequency	3.5
Intermediate frequency	0.4
High frequency	0.08

where P_0 (kN) is the total weight of the vibration source and P_1 (kN) is the vibration load peak corresponding to the vibration source circular frequency ω_1.

The total weight of the vibration source is P_0 = 100 kN, and the expression of the peak vibration load P_1 is shown in Eq. (5):

$$P_1 = M_0 \alpha_1 \omega_1 \tag{5}$$

where α_1 (mm) is the amplitude corresponding to the vibration source circular frequency ω_1 and M_0 (kg) is the mass of the vibration source.

The mass of the vibration source is M_0 = 750 kg, and the vibration wave amplitude α_1 in different frequency ranges is shown in Table 4. The expression of the circular frequency ω_1 is shown in Eq. (6):

$$\omega_1 = 2\pi f \tag{6}$$

where f (Hz) is the vibration wave frequency.

The low, intermediate and high frequencies are represented by 10 Hz, 50 Hz and 120 Hz, respectively. The low-, intermediate- and high-frequency vibration functions are given by Eqs. (7), (8) and (9), respectively:

$$F(t) = 100 + 10.35 \sin(62.8t) \tag{7}$$

$$F(t) = 100 + 29.58 \sin(314.0t) \tag{8}$$

$$F(t) = 100 + 34.07 \sin(753.6t) \tag{9}$$

4.2 Schematic Design

This study changes the number of piles, pile depth, pile spacing, pile shape, vibration source to row pile distance and source vibration frequency. The influence of different factors on the vibration isolation of row piles is studied by generating an Ar contour map. The smaller the Ar value behind the row piles is, the better the vibration isolation effect. The specific scheme is shown in Table 5.

Experiment nos. 0–1 to 0–5 are isolation tests without vibration. Because the row piles are noncontiguous vibration isolation barriers, the relative locations of the vibration source and the row piles are divided into two situations: the vibration source directly opposite the pile center and the vibration source directly between two piles. A schematic diagram is shown in Fig. 6.

Table 5 Test plan table

Test number	Number of piles	Pile depth (m)	Pile spacing (m)	Pile shape	Vibration source to row pile distance (m)	Source vibration frequency (Hz)	Vibration source location
0–1	0	–	–	–	1	10	–
0–2	0	–	–	–	3	10	–
0–3	0	–	–	–	5	10	–
0–4	0	–	–	–	3	50	–
0–5	0	–	–	–	3	120	–
1	1	10	1.0	Solid square	3	10	Pile center
2	2	10	1.0	Solid square	3	10	Between two piles
3	3	10	1.0	Solid square	3	10	Pile center
4	4	10	1.0	Solid square	3	10	Between two piles
5	14	10	1.0	Solid square	3	10	Between two piles
6	15	10	1.0	Solid square	3	10	Pile center
7	14	5	1.0	Solid square	3	10	Between two piles
8	15	5	1.0	Solid square	3	10	Pile center
9	14	15	1.0	Solid square	3	10	Between two piles
10	15	15	1.0	Solid square	3	10	Pile center
11	14	10	0.5	Solid square	3	10	Between two piles
12	15	10	0.5	Solid square	3	10	Pile center
13	14	10	1.5	Solid square	3	10	Between two piles
14	15	10	1.5	Solid square	3	10	Pile center
15	14	10	1.0	Hollow square	3	10	Between two piles
16	15	10	1.0	Hollow square	3	10	Pile center
17	14	10	1.0	Solid circle	3	10	Between two piles
18	15	10	1.0	Solid circle	3	10	Pile center

(continued)

Table 5 (continued)

Test number	Number of piles	Pile depth (m)	Pile spacing (m)	Pile shape	Vibration source to row pile distance (m)	Source vibration frequency (Hz)	Vibration source location
20	15	10	1.0	Solid square	1	10	Pile center
21	14	10	1.0	Solid square	5	10	Between two piles
22	15	10	1.0	Solid square	5	10	Pile center
23	14	10	1.0	Solid square	3	50	Between two piles
24	15	10	1.0	Solid square	3	50	Pile center
25	14	10	1.0	Solid square	3	120	Between two piles
26	15	10	1.0	Solid square	3	120	Pile center

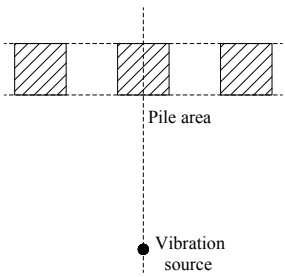

(a) Vibration source directly opposite the pile center

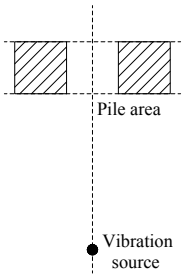

(b) Vibration source directly between two piles

Fig. 6 Relative locations of the vibration source and the row piles

5 Analysis of the Results

5.1 Analysis of the Acceleration Characteristics of Row Pile Vibration Isolation

To study and analyze the characteristics of the vibration propagation from vibration excitation at a single point and the principle of the vibration isolation of row piles, contour maps of acceleration were drawn for situations with and without row pile vibration isolation. No vibration isolation was used in test no. 0–2, and row pile vibration isolation was used in test no. 6. The data acquisition interval is 1 m, and a total of 441 measurement point data were collected. The acceleration contours from test no. 0–2 are shown in Fig. 7. The acceleration contours for test no. 6 are shown in Fig. 8.

As shown in Fig. 7, in the absence of vibration isolation, the vibration wave is centered on the excitation point and spreads outward. The acceleration is constantly attenuated as the distance increases. During the initial period, the acceleration decay rate is fast but gradually decreases as the distance increases. Finally, the acceleration gradually levels off and slowly approaches zero.

As shown in Fig. 8, the acceleration diffuses to the periphery behind the row pile vibration isolation. Acceleration near the excitation point is greater than that in the isolation case without vibration, and the rate of acceleration decay increases. At the same time, the acceleration in the area far from the excitation point is considerably less than that in the isolation case without vibration.

To further analyze the acceleration attenuation characteristics of row pile vibration isolation, the profile line L1 passing through the excitation point and parallel to the *y*-axis was used as the reference line to create an acceleration profile. The results are shown in Figs. 9 and 10.

As shown in Fig. 9, the vibration point is located at 2 m, and the acceleration is 2.553 m/s^2. As the distance from the excitation point increases, the acceleration and the acceleration attenuation rate decrease. The acceleration decreases most rapidly at distances from 2 to 3 m, and the acceleration is 0.774 m/s^2 at 3 m. The acceleration decreased by 1.279 m/s^2 compared to that of the excitation point, corresponding to approximately 62.30% of the acceleration at the excitation point. From 3 to 6 m, the rate of acceleration decay gradually decreases, with the acceleration at 6 m being 0.162 m/s^2, corresponding to 29.84% of the acceleration at the excitation point. From 6 to 20 m, the acceleration decays slowly and gently, and the acceleration is reduced to 7.72% of that at the excitation point.

As shown in Fig. 10, the excitation point is located at 2 m, and the row piles are arranged in the range from 5 to 6 m. Compared with the isolation case without vibration, the case with row piles features greater acceleration near the excitation point because the row piles reflect the vibration wave; however, the acceleration attenuation is more rapid. The acceleration at the excitation point is 2.278 m/s^2, which is 10.96% higher than that without vibration isolation. From 2 to 6 m, the

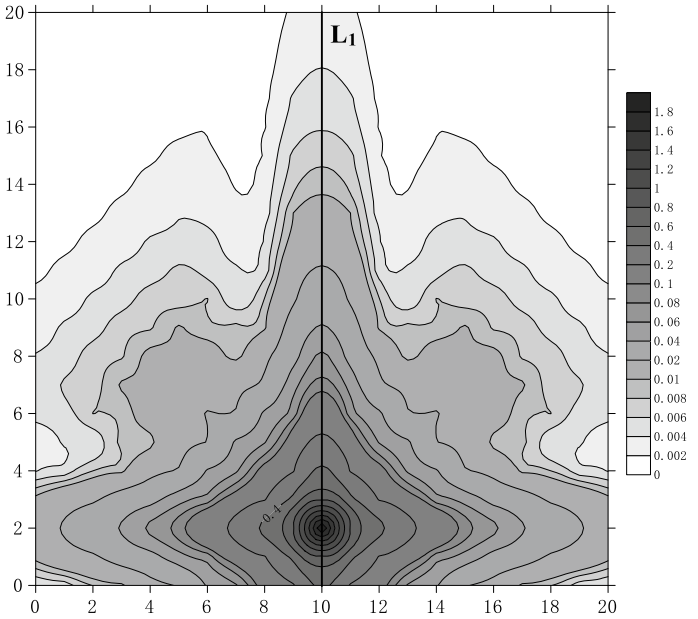

Fig. 7 Acceleration contour map for test no. 0–2

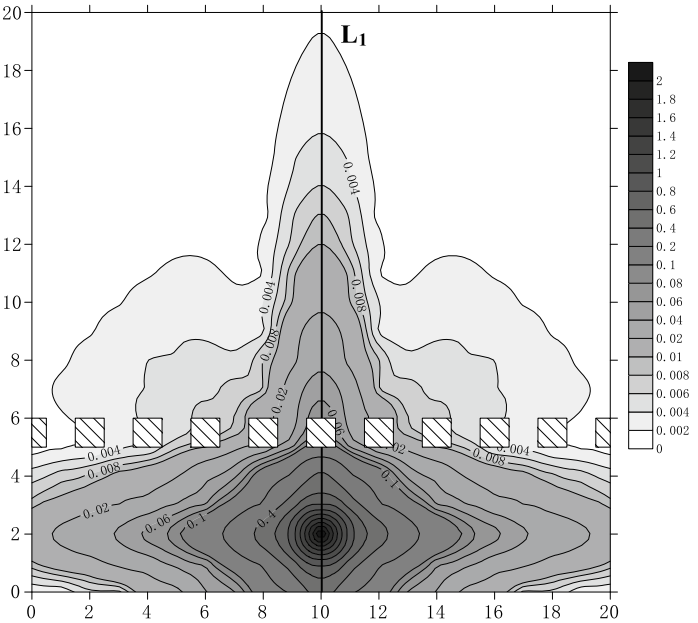

Fig. 8 Acceleration contour map for test no. 6

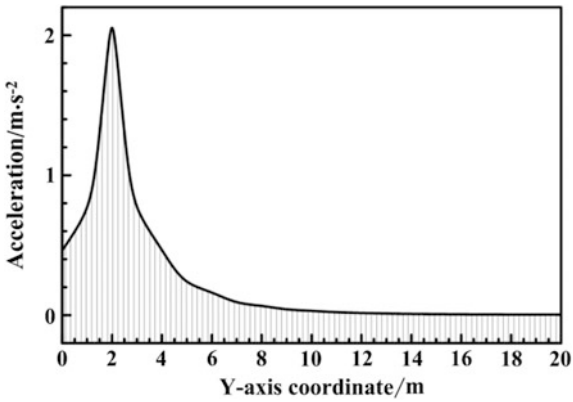

Fig. 9 Acceleration profile for line L1 in test no. 0–2

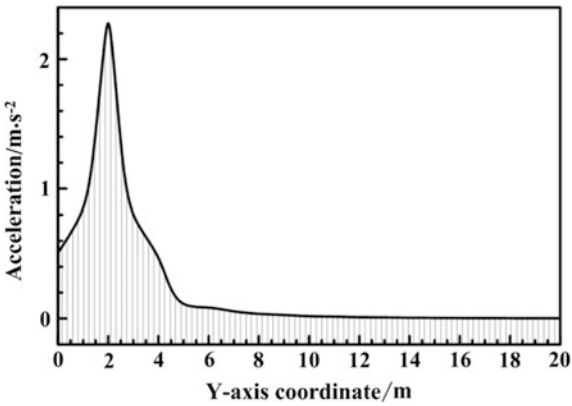

Fig. 10 Acceleration profile for line L1 in test no. 6

acceleration decays rapidly, with an acceleration at 6 m of 0.084 m/s^2, corresponding to 96.30% of that at the excitation point. The acceleration is 47.78% lower than that at the same position in the isolation case without vibration, meaning that the row piles had an obvious vibration isolation effect. From 5 to 20 m, the acceleration slowly declines with a gentle trend, and the acceleration reaches 3.62% of that at the excitation point.

To further study the acceleration change induced by the row piles, acceleration results at each point in test no. 6 are divided by those at each point in test no. 0–1 to obtain the *Ar* value at each point and to draw an *Ar* contour map. The results are shown in Fig. 11.

Figure 11 shows that, in front of the row piles and especially in the area near the middle line, the *Ar* in most areas is greater than 1.0 because the vibration wave reflects off the row piles. Behind the row piles, the *Ar* values are between 0.3 and 0.7, which represents a good vibration isolation effect. In particular, in the area far from the midline, *Ar* is 0.3–0.4, and the vibration isolation effect is good. *Ar* near

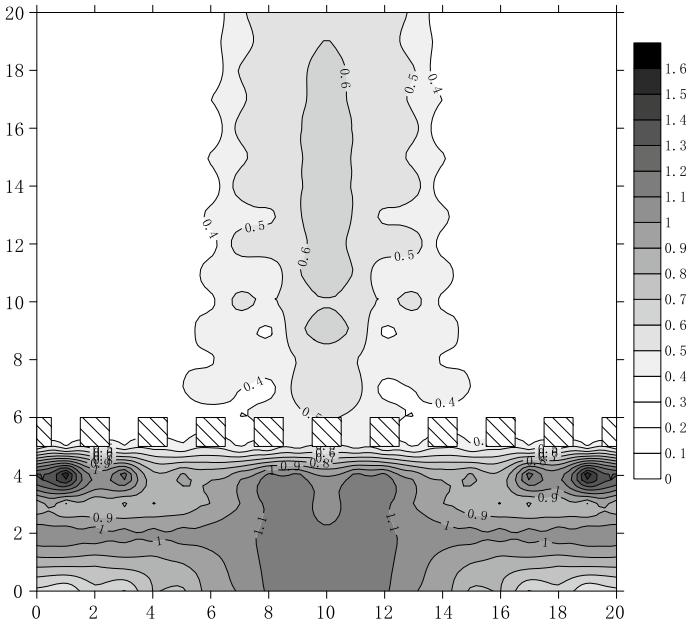

Fig. 11 Comparison of acceleration between test no. 6 and test no. 0–1

the midline area is 0.4–0.7. This finding reveals that areas closer to the midline exhibit larger *Ar* values. The convergence of diffracted waves causes large *Ar* values from 0.6 to 0.7.

5.2 *Influence of the Row Pile Parameters on the Vibration Isolation Effect*

5.2.1 Number of Row Piles

Next, we examined the effect of the numbers of row piles on the vibration isolation effect. Using a single pile (test no. 1), two piles (test no. 2), three piles (test no. 3), four piles (test no. 4), a row of piles (test no. 5 and no. 6) and a test without isolation (test no. 0–2), *Ar* contour maps were created and analyzed. The results are shown in Figs. 12, 13, 14, 15, 16 and 17. The squares filled with cross-hatching show the arrangement of the row piles.

From Figs. 12, 13, 14, 15, 16 and 17, we see that the vibration isolation effect becomes more obvious as the number of row piles increases. For vibration isolation using a single pile, the vibration isolation effect is good on both sides of the pile and in the rear area. *Ar* is essentially less than 0.6, and part of the area behind the single pile reaches values less than 0.5. In the vibration isolation case using two piles, the

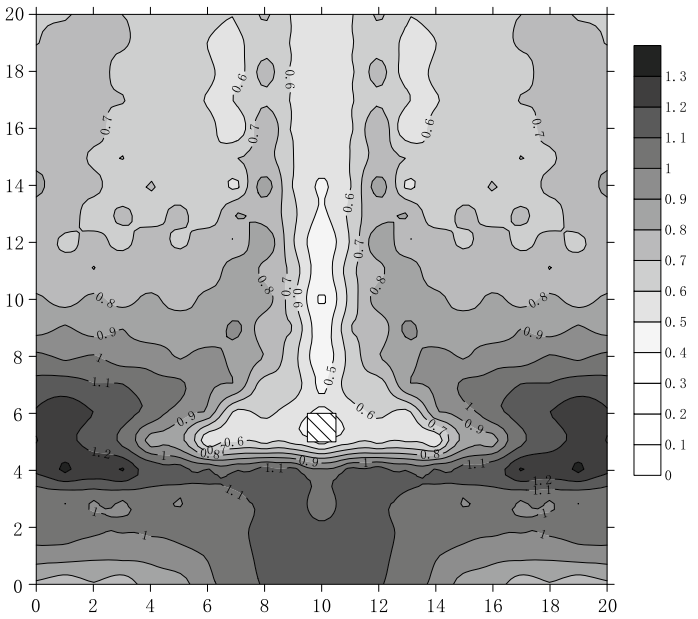

Fig. 12 Test no. 1 *Ar* contour map

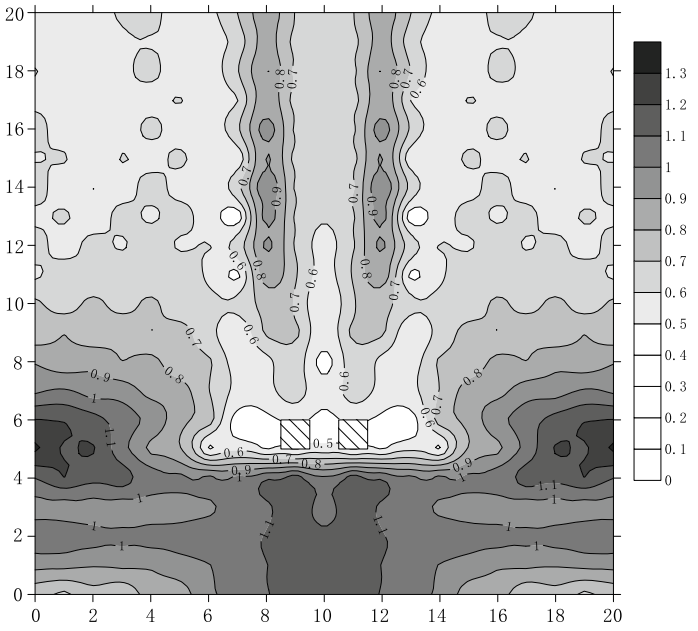

Fig. 13 Test no. 2 *Ar* contour map

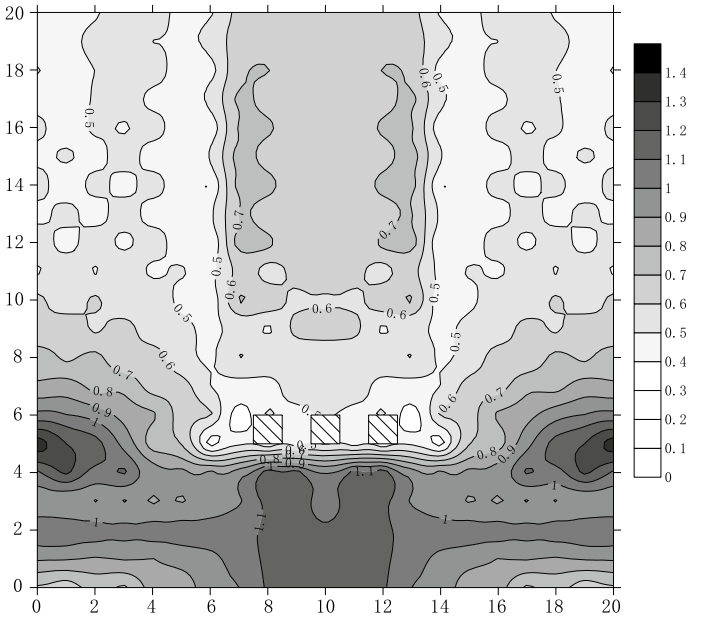

Fig. 14 Test no. 3 *Ar* contour map

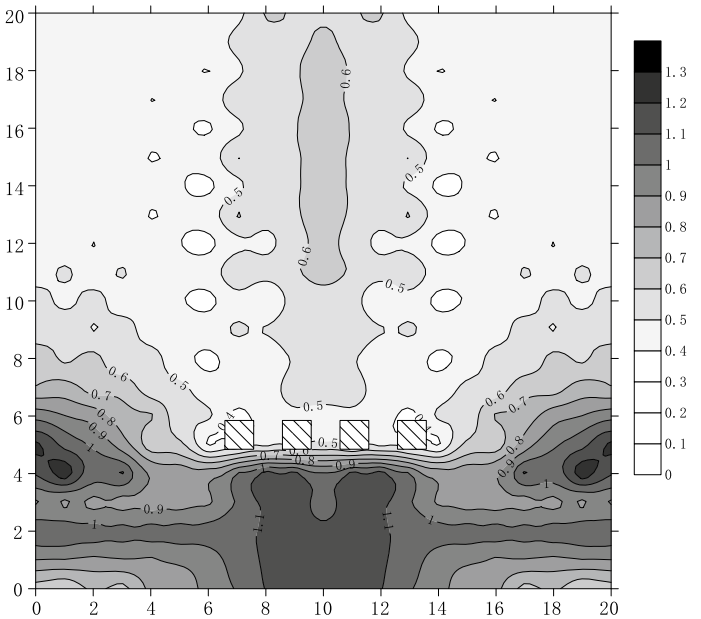

Fig. 15 Test no. 4 *Ar* contour map

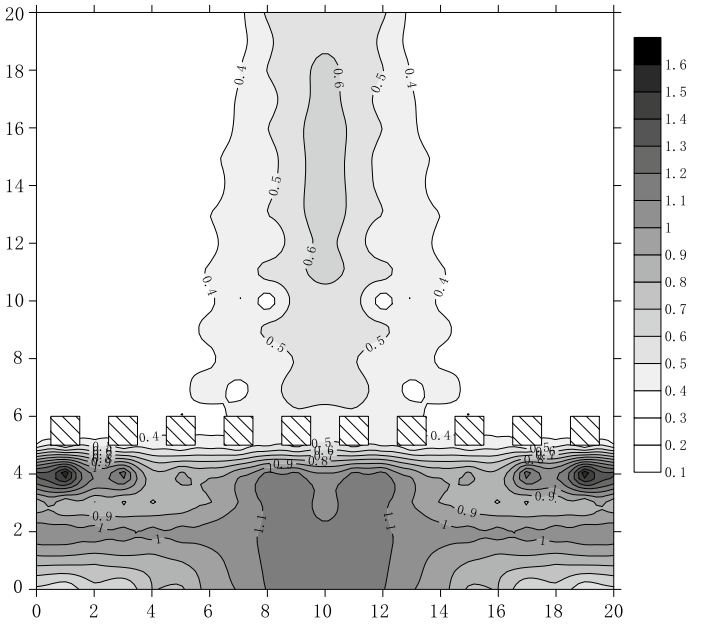

Fig. 16 Test no. 5 *Ar* contour map

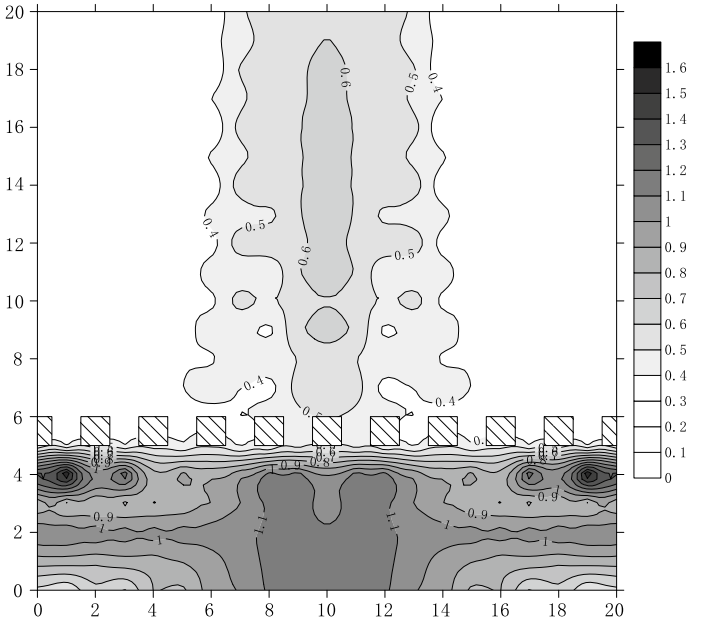

Fig. 17 Test no. 6 *Ar* contour map

areas between and on both sides of the two piles experience the best vibration isolation effect, and the middle-rear area of the two piles also sees positive effects. However, poor isolation is observed immediately behind the two piles. For the vibration isolation case using three piles, there is a poor vibration isolation effect in the rear area but a good vibration isolation effect on both rear sides. In the vibration isolation case using four piles, the vibration isolation effect is similar to but slightly worse than that for a row of piles. The vibration isolation effect is good on both sides of the isolation piles, but the isolation effect on the rear side of the isolation piles is poor. For the vibration isolation case using a row of piles, the overall vibration isolation effect is the same regardless of whether the vibration source is directly opposite the pile center or the vibration source is directly between the two piles. Behind the row of piles, the vibration isolation effect on both sides is better than that in the middle area. In addition, the vibration isolation effect when the vibration source is directly between the two piles is slightly better than that when the vibration source is directly opposite the pile center.

5.2.2 Pile Depth

Next, we studied the effect of different pile depths on the vibration isolation effect. Depths of 5 m (tests no. 7 and no. 8), 10 m (tests no. 5 and no. 6), 15 m (tests no. 9 and no. 10) and a test without isolation (test no. 0–2) were used to draw *Ar* contour maps, which were then analyzed. The results are shown in Figs. 16, 17, 18, 19, 20 and 21.

From Figs. 16, 17, 18, 19, 20 and 21, we see that the trend for the vibration isolation effect is generally the same, and a vibration superposition enhancement region appears in the front of the row piles. The overall vibration isolation effect in the rear of the row piles is good, and the vibration isolation effect on both sides of the row piles was better than that in the middle area. This pattern is observed because of vibration wave convergence in the middle. In addition, the vibration isolation effect when the vibration source is directly between the two piles is slightly better than that when the vibration source is directly opposite the pile center.

Figures 18 and 19 show *Ar* contour maps constructed at a 5 m depth. Compared with the case with a 10 m row depth, the case with a 5 m row depth features areas with worse vibration isolation effects on both sides and in the middle. In general, the vibration isolation effect at a row depth of 5 m is worse than that at a depth of 10 m.

Figures 20 and 21 show *Ar* contour maps constructed at a 15 m depth. The area with poor vibration isolation in this case is smaller than that in the case with a 10 m depth. In general, the vibration isolation effect for a row depth of 15 m is better than that for a row depth of 10 m, but the difference is not large.

In summary, the vibration isolation effect increases as the depth of the row piles increases, but the ability to increase the vibration isolation effect decreases as the depth of the row piles increases.

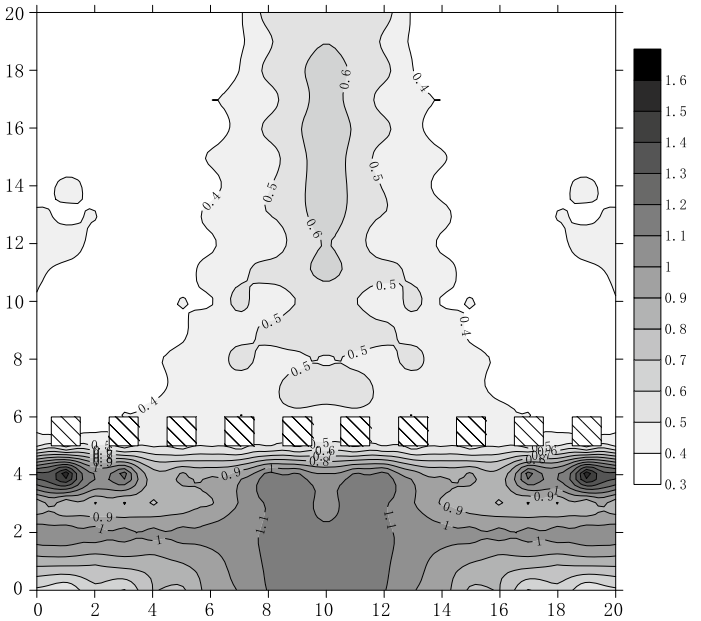

Fig. 18 Test no. 7 *Ar* contour map

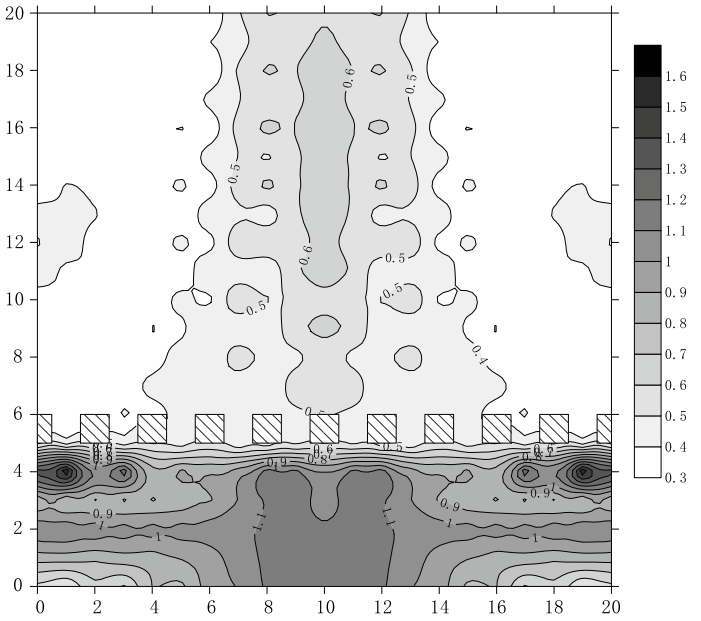

Fig. 19 Test no. 8 *Ar* contour map

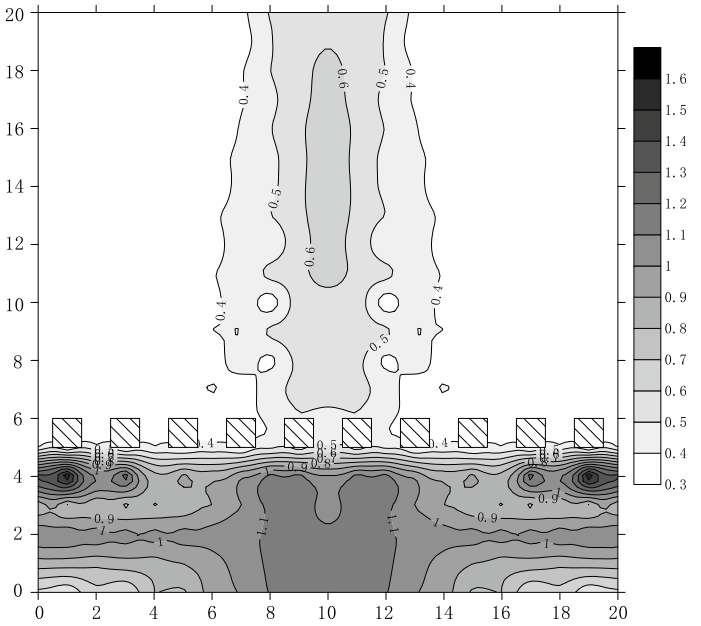

Fig. 20 Test no. 9 *Ar* contour map

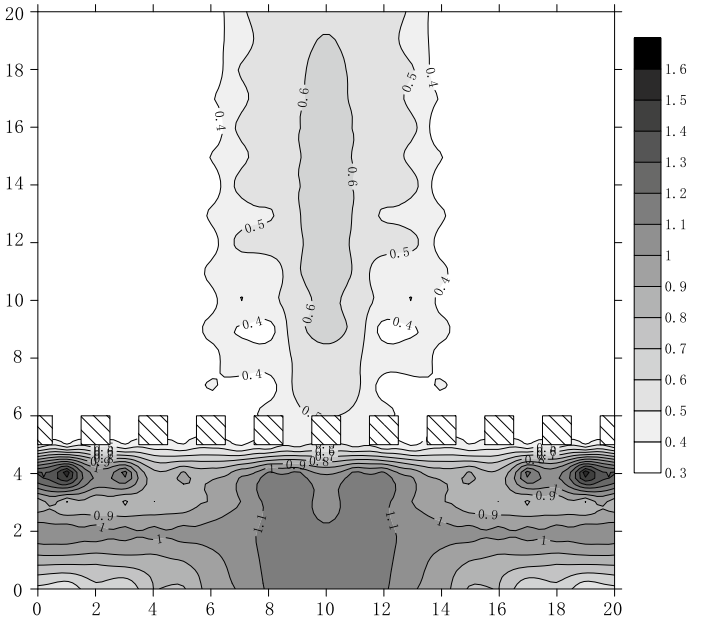

Fig. 21 Test no. 10 *Ar* contour map

5.2.3 Pile Spacing

Next, we investigated the effect of pile spacing on the vibration isolation effect using a spacing of 0.5 m (tests no. 11 and no. 12), a spacing of 1 m (tests no. 5 and no. 6), a spacing of 1.5 m (tests no. 13 and no. 14) and a test without isolation to construct and analyze *Ar* contour maps. The results are shown in Figs. 16, 17, 22, 23, 24 and 25.

From Figs. 16, 17, 22, 23, 24 and 25, we see that the vibration isolation effect changes greatly with the pile spacing and that the vibration wave superposition area appears in front of the row piles. When the pile spacing is 0.5 or 1.0 m, the isolation effect of the row piles is generally good. However, when the pile spacing is 1.5 m, there is a large area with poor isolation behind the row piles.

Figures 22 and 23 show *Ar* contour maps for a pile spacing of 0.5 m. Compared with a pile spacing of 1.0 m, the pile spacing of 0.5 has a larger area with an *Ar* of 0.6 and a smaller area with an *Ar* of 0.4. However, this pile spacing also has a larger area with an *Ar* between 0.5 and 0.6. When the vibration source is between two piles, there are several small areas with *Ar* values greater than 0.8 and an area with *Ar* values of less than 0.4 alternating with *Ar* values from 0.4 to 0.5. When the vibration source is directly opposite the pile center, only three small areas at the midline feature *Ar* values greater than 0.6; however, the area with *Ar* values of 0.4–0.5 is considerably larger.

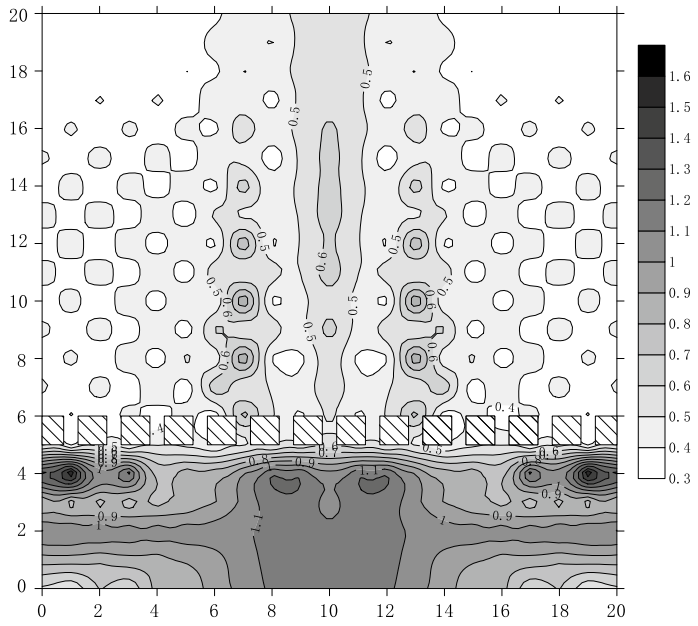

Fig. 22 Test no. 11 *Ar* contour map

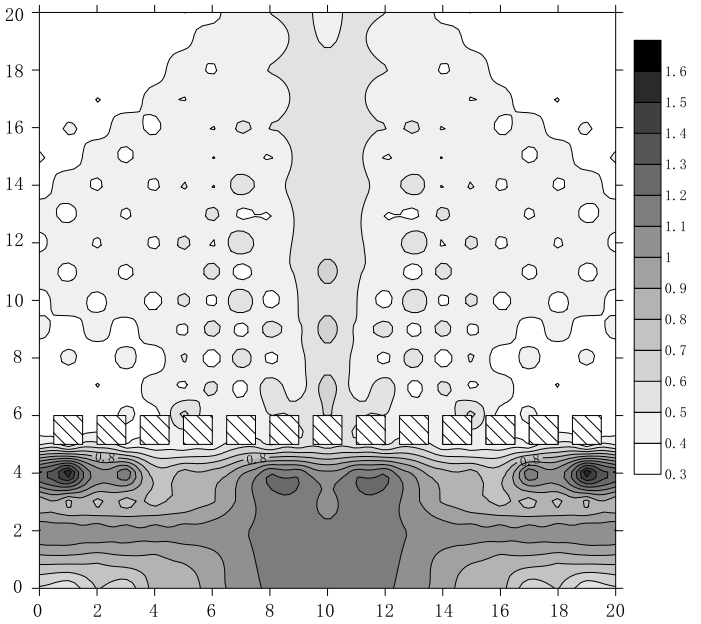

Fig. 23 Test no. 12 *Ar* contour map

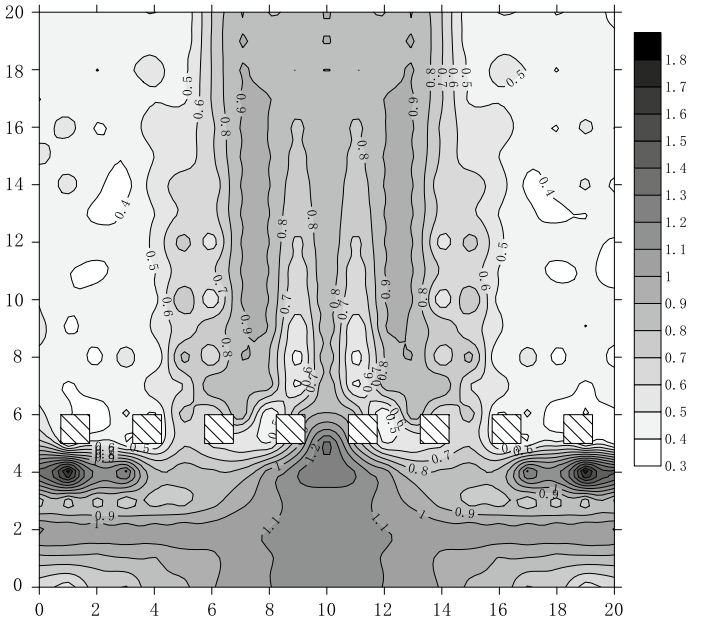

Fig. 24 Test no. 13 *Ar* contour map

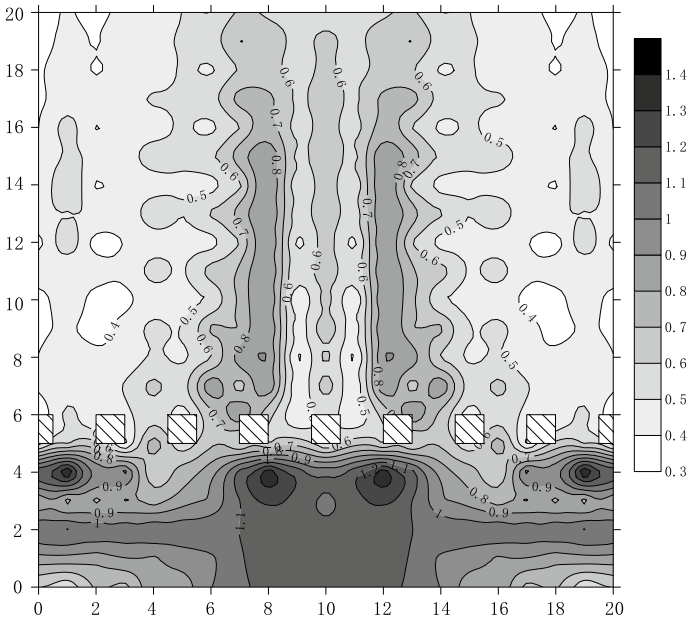

Fig. 25 Test no. 14 *Ar* contour map

Figures 24 and 25 show *Ar* contour maps for a pile spacing of 1.5 m. Compared with a pile spacing of 1.0 m, the pile spacing of 1.5 m is associated with few areas that have an *Ar* value less than 0.4, and an area where *Ar* is greater than 0.8 is present in the middle. When the vibration source is between two piles, the area with poor vibration isolation expands to the rear in an inverted triangle shape. Large areas with poor vibration isolation exhibit *Ar* values greater than 0.9. The overall vibration isolation effect is poor. When the vibration source is directly opposite the pile center, the overall trend is similar to that when the vibration source is between two piles. However, when the vibration source is directly opposite the pile center, the overall *Ar* value is lower by 0.1–0.2, and the vibration isolation effect is slightly better than that when the vibration source is between two piles but is still poor compared to that with a pile spacing of 1.0 m.

In summary, changing the pile spacing greatly impacts the vibration isolation effect of row piles. Excessive pile spacing will cause an unsatisfactory vibration isolation effect but reducing the pile spacing may not improve the vibration isolation effect.

5.2.4 Pile Shape

To examine the effect of pile shape on the vibration isolation effect, we tested hollow square piles (tests no. 15 and no. 16), solid square piles (tests no. 5 and no.

6), solid circular piles (tests no. 17 and no. 18) and a test without isolation (test no. 0–2) to construct and analyze *Ar* contour maps. The results are shown in Figs. 16, 17, 26, 27, 28 and 29.

From Figs. 16, 17, 26, 27, 28 and 29, we see that the overall trend for the vibration isolation effect of hollow square piles is similar to that of solid square piles. In contrast, the overall trend of vibration isolation for solid circular piles is different from that of square solid piles. Square row piles (both solid and hollow) have a better vibration isolation effect than circular piles of the same diameter.

Figures 26 and 27 show *Ar* contour maps for hollow square piles. Compared with the case with solid square piles, the case with hollow square piles has vibrations that are superimposed at the rear of the row piles and offset to both sides when the vibration source is directly between two piles; the area corresponding to *Ar* 0.4–0.7 is greater, and a number of small and discontinuous areas with *Ar* 0.7–0.8 are present. Overall, the vibration isolation effect of the hollow square piles is slightly worse than that of the solid square piles. When the vibration source is directly opposite the pile center, the vibration superposition area at the rear of the row piles shifts backward, but the area is approximately the same. The area corresponding to *Ar* 0.5–0.6 shifts backward and decreases slightly. However, the area corresponding to *Ar* 0.4–0.5 decreases in the rear and increases in the front, resulting in an overall increase in area. Overall, the vibration isolation effect is slightly worse for the hollow square piles than for the solid square piles.

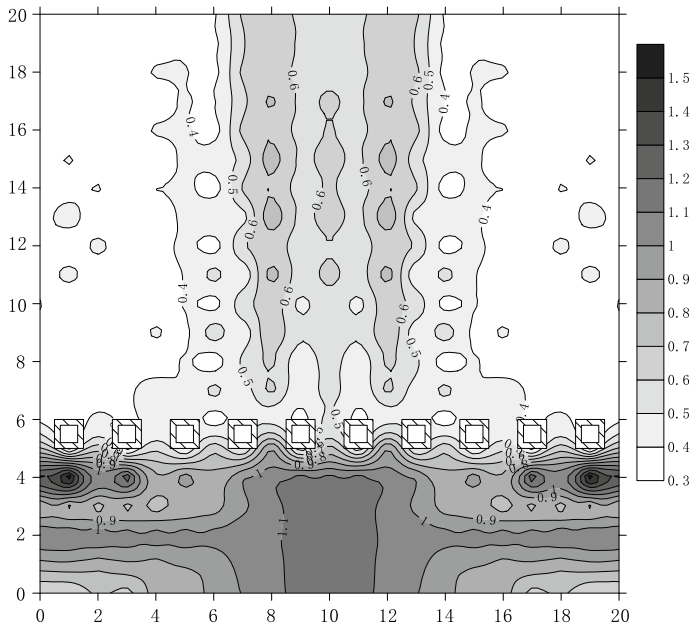

Fig. 26 Test no. 15 *Ar* contour map

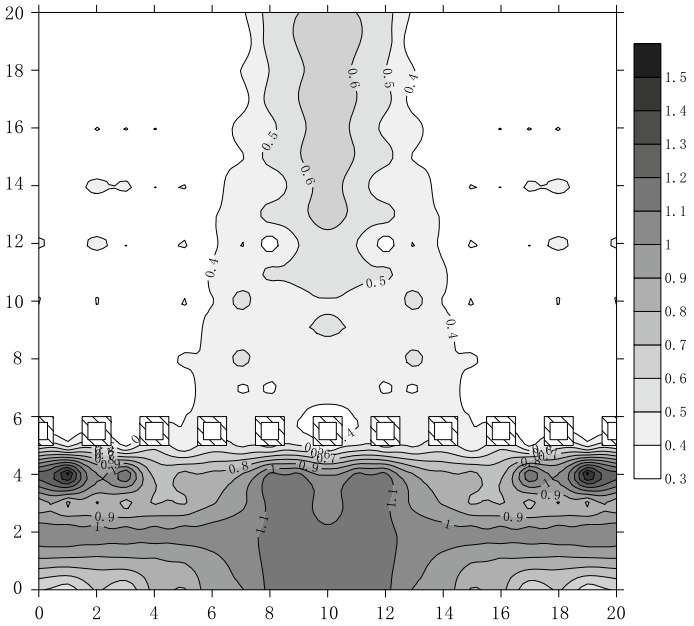

Fig. 27 Test no. 16 *Ar* contour map

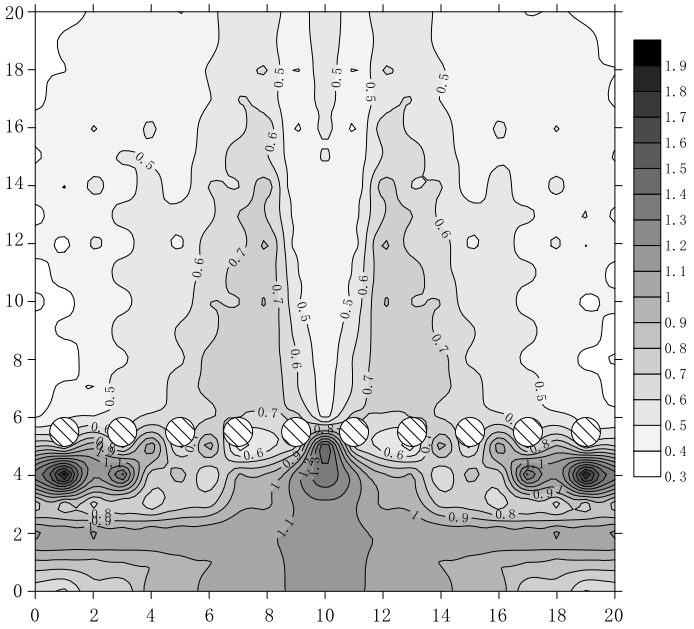

Fig. 28 Test no. 17 *Ar* contour map

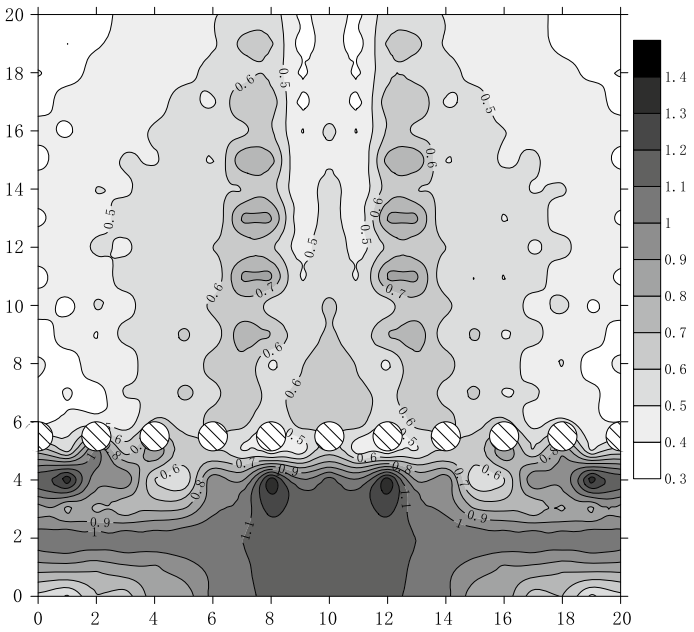

Fig. 29 Test no. 18 *Ar* contour map

Figures 28 and 29 show the *Ar* contour maps for solid circular piles. When the vibration source is directly between the two piles, the vibration superposition area appears on both sides and in the middle of the front part of the row pile. An area of *Ar* 0.5–0.6 appears in the middle of the area behind the row piles, an area of *Ar* 0.7–0.8 appears on both sides of the row piles, and the *Ar* gradually decreases on both sides. When the vibration source is directly opposite the pile center, *Ar* values of 0.6 or greater appear on both sides of the area behind the row pile, and the *Ar* values gradually decrease as the vibration propagates.

In summary, hollow piles have a better vibration isolation effect than solid piles, but vibration isolation effects are not significantly different. However, circular piles of the same diameter are less effective than square piles.

5.2.5 Vibration Source Location

Next, we studied the effect of vibration source location on the vibration isolation effect using distances between the vibration source and the row piles of 1 m (tests no. 19 and no. 20), 1 m (test no. 5 and no. 6), 1 m (test no. 21 and no. 22) and tests without isolation (tests no. 0–1, no. 0–2 and no. 0–3) to construct and analyze *Ar* contour maps. The results are shown in Figs. 16, 17, 30, 31, 32 and 33.

From Figs. 16, 17, 30, 31, 32 and 33, we see that the vibration isolation effects are similar. An area of superimposed vibration behind the row piles appears in the

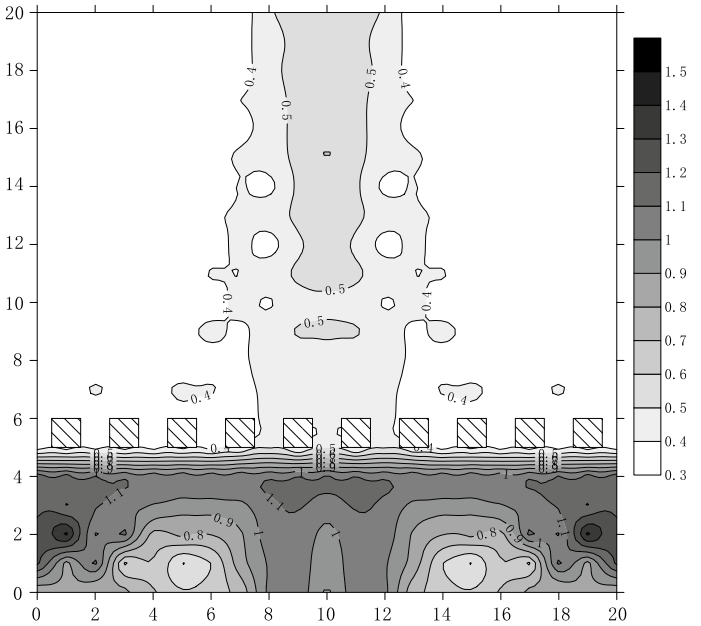

Fig. 30 Test no. 19 *Ar* contour map

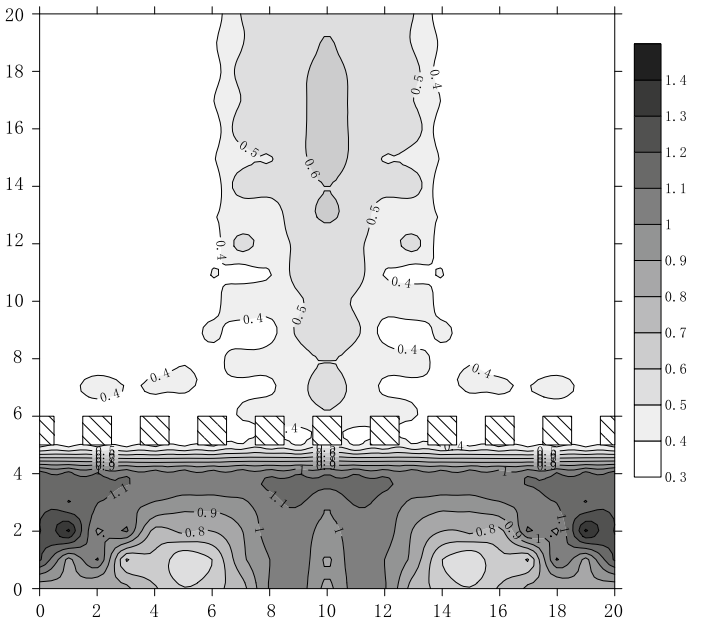

Fig. 31 Test no. 20 *Ar* contour map

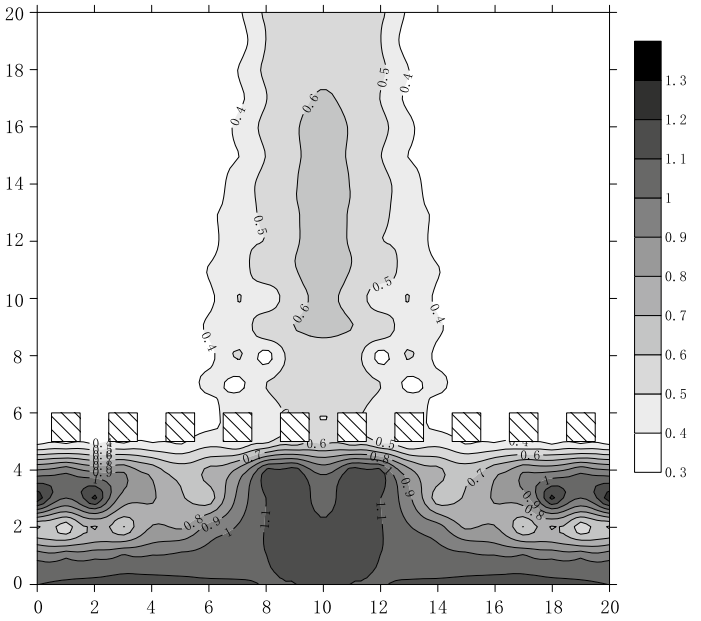

Fig. 32 Test no. 21 *Ar* contour map

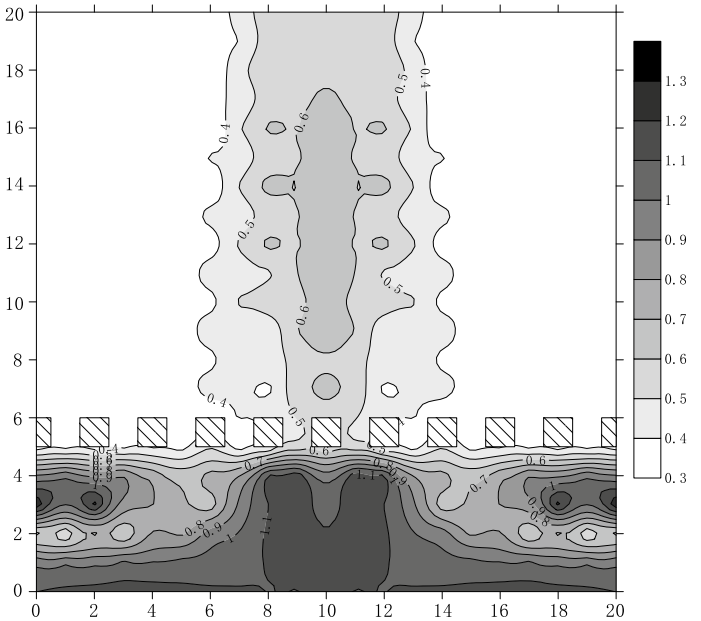

Fig. 33 Test no. 22 *Ar* contour map

middle in all cases. The vibration isolation effect at both sides is more pronounced than that in the middle area.

Figures 30 and 31 show *Ar* contour maps for a vibration source distance from the row piles of 1 m. Compared with a vibration source distance from the row pile of 3 m, a vibration source distance from the row piles of 1 m is associated with a vibration wave superposition area in front of the row piles that has shifted backward and *Ar* values in the middle area that have decreased to slightly above 1.1. The area where *Ar* is greater than 0.4 in the rear of the row piles is reduced. In general, the vibration isolation effect of a vibration source distance of 1 m is better than that of a vibration source distance of 3 m, but the difference is not significant.

Figures 32 and 33 show *Ar* contour maps for a vibration source distance from the row piles of 5 m. Compared with a vibration source at a 3 m distance from the row pile, a vibration source distance from the row piles of 5 m is associated with a vibration wave superposition area in front of the row piles that has shifted backward and *Ar* values in the middle area that have increased to slightly above 1.0. Behind the row piles, the area where *Ar* is greater than 0.4 is approximately the same, but the area where *Ar* is greater than 0.6 is larger. In general, the vibration isolation effect for a vibration source distance of 5 m is worse than for a vibration source distance of 3 m, but the difference is not significant.

In summary, the vibration isolation effect improves as the distance from the source to the row piles decreases, but the differences are not significant.

5.2.6 Vibration Source Frequency

Finally, we examined the effect of vibration source frequency on the vibration isolation effect using a low-frequency vibration (10 Hz, tests no. 5 and no. 6), an intermediate-frequency vibration (50 Hz, tests no. 23 and no. 24), a high-frequency vibration (120 Hz, tests no. 25 and no. 26) and tests without isolation (tests no. 0–2, no. 0–4 and no. 0–5) to construct and analyze *Ar* contour maps. The results are shown in Figs. 16, 17, 34, 35, 36 and 37.

From Figs. 16, 17, 34, 35, 36 and 37, we see that the vibration isolation effects tend to be similar for intermediate- and high-frequency vibrations but are significantly different for low-frequency vibrations. For intermediate- and high-frequency vibrations, the vibration isolation effect behind the row piles is not ideal.

Figures 34 and 35 show *Ar* contour maps for a vibration source frequency of 50 Hz. The area where the *Ar* is greater than 1.0 is large behind the row piles; there are even small areas where the *Ar* value is greater than 1.5. As the distance from the row piles increases, *Ar* gradually decreases, and the area where *Ar* is less than 0.2 appears far from the row piles.

Figures 36 and 37 show *Ar* contour maps for a vibration source frequency of 120 Hz. The *Ar* pattern behind the row piles for the high-frequency vibration is similar to that for the intermediate-frequency vibration. However, the rate of decrease in *Ar* is greater for high-frequency vibration than for intermediate-frequency vibration. Overall, the vibration isolation effect of the row

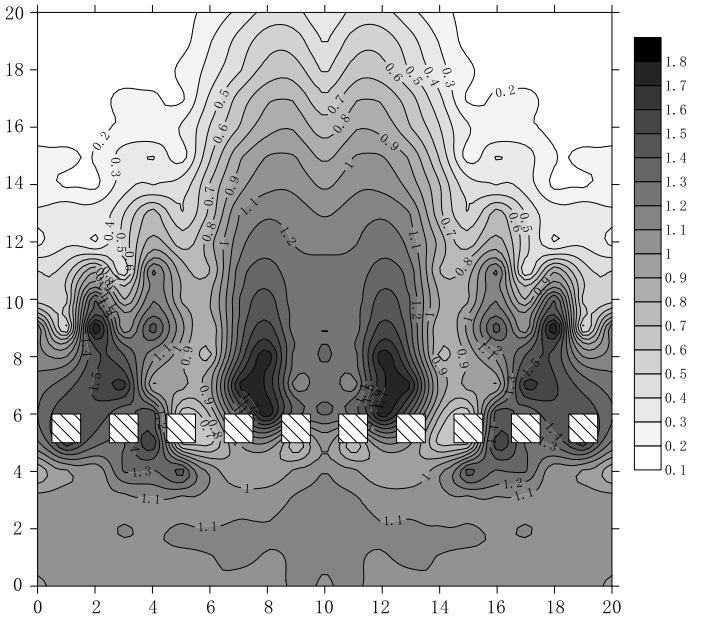

Fig. 34 Test no. 23 *Ar* contour map

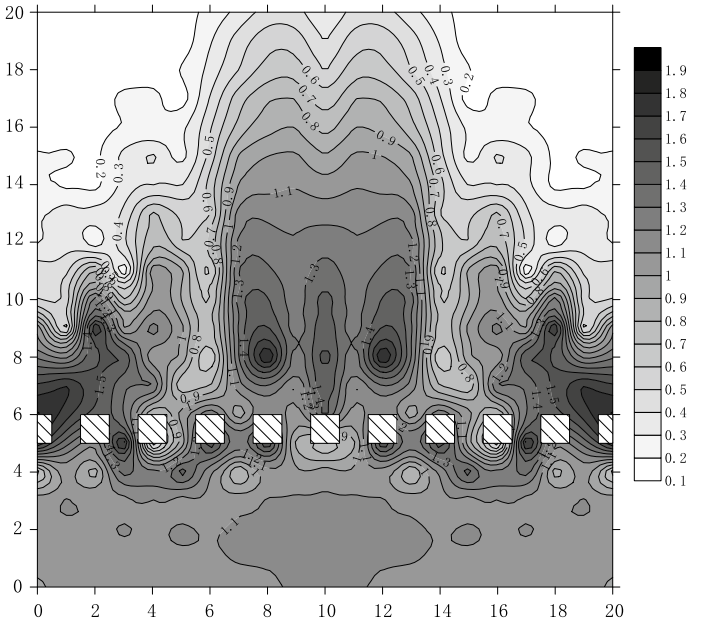

Fig. 35 Test no. 24 *Ar* contour map

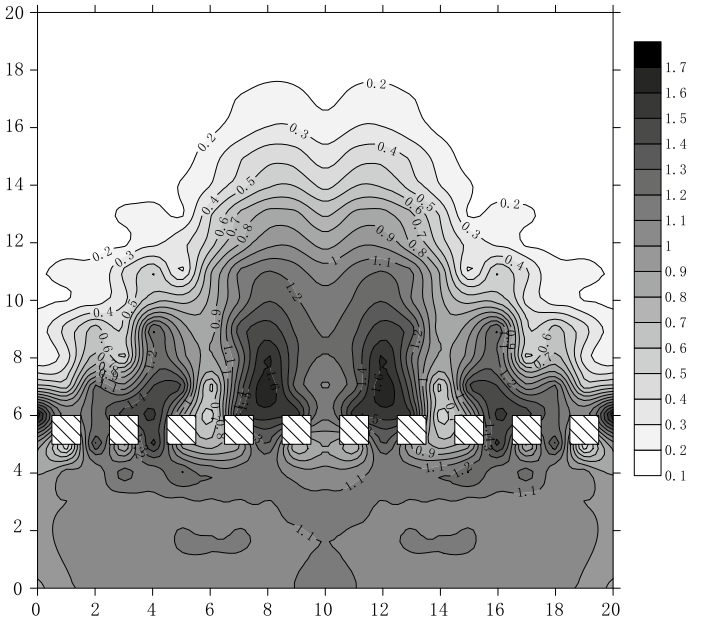

Fig. 36 Test no. 25 *Ar* contour map

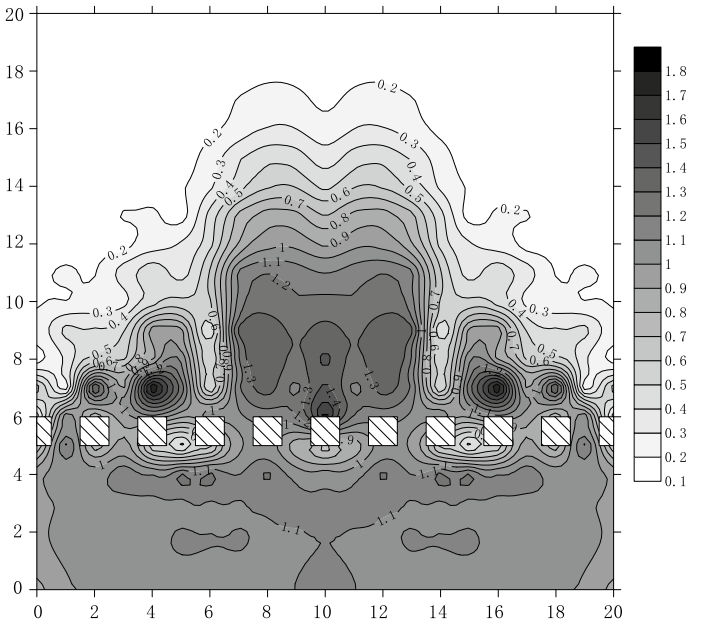

Fig. 37 Test no. 26 *Ar* contour map

piles for a high-frequency vibration is slightly better than that for an intermediate-frequency vibration.

In summary, row piles are not ideal for vibration isolation of high- and intermediate-frequency vibrations but exhibit good vibration isolation effects for low-frequency vibrations.

6 Analysis of the Results

In this work, a finite element model of a foundation with an infinite element boundary was established based on the theory of an elastic half-space body. The model included a single-point vibration source in the free field and piles arranged in a row. The results were used to construct contour maps of the amplitude dissipation ratio (Ar) with respect to cases without vibration isolation. The conclusions from this work are as follows:

(1) A finite element model using infinite element boundaries can effectively reflect the actual effects of vibration isolation measures.
(2) Radial vibration waves propagate from the excitation point, and their acceleration amplitudes continuously decay until they eventually stabilize. The row pile vibration isolation increases the acceleration in front of the row piles and reduces the acceleration behind the row piles.
(3) The vibration isolation effect increases with the number of vibration isolation piles. The vibration isolation effect increases as the depth of the row piles increases but only up to a point. Excessive pile spacing produces an unsatisfactory vibration isolation effect, but reducing the pile spacing may not improve the vibration isolation effect. Hollow piles have a better vibration isolation effect than solid piles but not significantly. Circular piles with the same diameter as square piles are more effective. The vibration isolation effect increases as the distance between the source and the row piles decreases, but the increase is not significant. Row piles are not ideal for vibration isolation of high- and intermediate-frequency vibrations but do produce a good vibration isolation effect for low-frequency vibrations.

References

1. Ahmad S, Al-Hussaini TM, Fishman KL (1996) Investigation on active isolation of machine foundations by open trenches. J Geotech Eng 122:454–461
2. Gao GY, Feng SJ, Li W (2007) 2-D analysis of vibration isolation by wave impeding block in layered ground. J Vib Eng 20(2):174–179
3. Gao GY, Wang F, Chen GQ (2014) Active vibration isolation of the saturated ground with wave impedance block inside and under the load of the travelling train. J Vib Eng 27(3):433–440

4. Yang XJ (1992) Soil dynamics in industrial environment vibration. Chin J Geotech Eng 14 (2):82–88
5. Deng YH, Xia TD, Chen JY (2007) Analysis of efficiency of vibration isolating groove subjected to vehicle load. Rock Soil Mech 5:883–887, 894
6. Xiao SW, Lei CS, Guo C (2011) Numerical analysis of vibration reduction of open trench for high-speed railway. J Railw Eng Soc 8:23–29
7. Yang XJ, Xu J, Zhang CH (2013) Soil–foundation vibration and vibration isolation, 1st edn. China Architecture & Building Press, Beijing
8. Woods RD (1968) Screening of surface waves in soil. J Solids Mech Found Div 94 (SM4):951–979
9. Andersen L, Nielsen SRK (2005) Reduction of ground vibration by means of barriers or soil improvement along a railway track. Soil Dyn Earthq Eng 25(7):701–716
10. Aviles J, Sanchez-Sesma FJ (1983) Piles as barriers for elastic waves. J Geotech Eng 109 (9):1133–1146
11. Aviles J, Sanchez-Sesma FJ (1988) Foundation isolation from vibration using piles as barrier. J Eng Mech 114(11):1854–1870
12. Hayakawa K (1992) Reduction effects of ballast mats and EPS blocks on ground vibration caused by train and its evaluation. Inter-Noise 4:233–240
13. Xu P, Zhou XM, Xia TD (2007) Discontinuous barrier used a row of elastic piles for incident elastic waves. J Vib Eng 20(4):388–395
14. Xia TD, Sun MM, Chen C (2011) An improved method for multiple scattering and isolation of horizontal shear wave using double row of elastic discontinuous barrier. Rock Soil Mech 32(8):2402–2408
15. Shi G, Gao GY (2010) Three-dimensional analysis of a row of piles as passive barriers in saturated soil. J Vib Eng 23(05):546–553
16. Ba ZN, Wang JY, Liang JW (2016) Reduction of train-induced vibrations by using a trench in a layered foundation. J Vib Eng 5:860–873
17. Chen F, Huang MS (2008) Isolation analysis of an annular in-filled trench against the environmental vibrations from a highway viaduct. J Vib Eng 21(3):241–247
18. Feng GS, Liu JL, Zhang RH (2017) Experimental research for influence of filling properties on vibration isolation effect of sand-filled trench. Railw Eng 57(02):151–155
19. Zhang LG, Liu JL, Hou EP (2017) Model test research on vibration isolation effects of filling barriers for railway subgrade. Railw Eng 04:146–150
20. Jiang JQ, Zhou HF, Zhang TQ (2004) Steady-state response of an elastic half-space under a moving point load. Chin J Geotech Eng 26(4):440–444